Journal of Smart Science and Technology

PENERBIT PRESS UNIVERSITI TEKNOLOGI MARA

2023 September Volume 2 Issue 3

eISSN: 2785-924X

Discovery of Inhibitors of MDM2 Against Nasopharyngeal Cancer: An *In-Silico* Investigation

Juliyan Gunasinghe[1], Muhammad Iqbal Abu Talib[1], Stephanie Cheah[1], Irine Runnie Ginjom[1], Lee Sue Han[1], Xavier Wezen Chee[1*]

[1] *Faculty of Engineering, Computing and Science, Swinburne University of Technology, Sarawak Campus, 93350 Kuching, Sarawak, Malaysia*

Received: 06-06-2023
Revised: 28-07-2023
Accepted: 10-08-2023
Published: 30-09-2023

*Correspondence
Email: xchee@swinburne.edu.my
(Xavier Wezen Chee)

DOI: https://doi.org/10.24191/jsst.v3i2.55

Abstract

Nasopharyngeal cancer is the fifth most common cancer among males in Malaysia between the ages of 25-59. Epstein-Barr virus is an established cause of nasopharyngeal cancer through an excess upregulation of Murine Double Minute 2 (MDM2). This study investigated potential lead candidates of MDM2 inhibitors by utilizing Molecular Docking and Molecular Dynamics Simulations with the existing drug database, DrugBank. Docking poses were predicted through GOLD molecular docking software utilizing GoldScore, ChemScore, and ChemPLP scoring functions; a consensus scoring was used, achieving an area under the receiver operating characteristic curve of 0.70. The top two compounds with high consensus docking scores, Venetoclax and Phaeophytin-B, were analyzed for binding stability through 250 ns of molecular dynamics simulation. Both Venetoclax and Phaeophytin-B showed good stability while posing favourable binding free energies of –50.46 kcal mol^{-1} and –50.86 kcal mol^{-1}, respectively. Additionally, our MM-GBSA calculations hinted that the interaction of Venetoclax and Phaeophytin-B with MDM2 is favoured through hydrophobic interactions – analogous to p53-MDM2 interactions. Our study proposes Venetoclax and Phaeophytin-B as potential chemical scaffolds that can be used for rational drug design of MDM2 inhibitors.

Keywords

Epstein-Barr virus; MM-GBSA; Molecular docking; Molecular dynamics

Citation: Gunasinghe, J., Abu Talib, M. I., Cheah, S., Ginjom, I. R., Lee, S. H., & Chee, X. W. (2023). Discovery of inhibitors of MDM2 against nasopharyngeal cancer: An *in-silico* investigation. *Journal of Smart Science and Technology*, *2*(3), 44-56.

1 Introduction

Nasopharyngeal cancer (NPC) is defined as a cancer in the epithelium of the nasopharynx region. Worldwide, NPC has an estimated 133,354 cases diagnosed in 2020[1]. Although rare in the Western-regions, significantly higher age-standardized rates can be found in East Asia, South-East Asia, and East Africa regions.

Nasopharyngeal cancer (NPC) is the fifth most common cancer among Malaysian males between the ages of 25-59 years old[1]. In Malaysia, 4,597 cases of NPC were reported between the period of 2012-2016, making it the fifth most common cancer among male Malaysians between the ages of 25-59 years old from 2012-2016[1]. In Sarawak, the males and females of the aboriginal Bidayuh have a risk of 2.3 and

1.9 fold, respectively, than the Sarawak average[2].

One of the causes of NPC is the Epstein-Barr virus (EBV) that upregulates Murine-Double-Minute 2 (MDM2)[3]. The Epstein-Barr virus (EBV) is a ubiquitous B-lymphotropic virus that is latently carried by all humans. IgA antibodies to EBV were detected years before the development of NPC and viral DNA and EBV antigen were detected in the epithelial cells of the nasopharynx region[4]. The consistent detection of EBV in NPC cases suggests EBV is a cofactor of NPC[5].

Under normal conditions, MDM2 and the tumor suppressor 53 protein (p53) regulate each other in a feedback loop. Upregulation of MDM2 by EBV virus causes an excess of MDM2 that ubiquitinates p53 and marks p53 for degradation. The disruption in this feedback loop affects the development of NPC[5].

It is also known that EBV can enhance MDM2 gene expression in NPC cell lines but only in cells that are able to express MDM2 genes and cannot activate MDM2 genes that are naturally expressed[5]. Moreover, EBV-transformed lymphoblastoid cell lines require suppression of p53 for growth transformation and survival achieved through MDM2 upregulation[6].

Restoring the p53's role as a tumor suppressor in the p53-MDM2 feedback loop emerges as a potential cancer therapeutic strategy. One of the ways that the p53-MDM2 feedback loop can be restored is through the inhibition of MDM2. MDM2 inhibitors already exist under preclinical, clinical investigation, and ongoing clinical trials. Two MDM2 inhibitors namely, Navtemadlin and Idasanutlin have shown strong *in-vivo* activity against EBV-positive B-cell lymphomas, with the activation of p53 pathways leading to tumor suppression[7].

NPC disproportionately affects Eastern-Asian regions, and current MDM2 inhibitors on the market are limited and still under clinical trials; targeting the p53-MDM2 pathways by downregulating MDM2 can result in the regulation and activation of p53 pathways[1,8].

Drug repurposing is a strategy for identifying new uses for approved or investigational drugs outside their original medical indication[9]. This strategy is a particularly advantageous search as repurposed drugs have already been found to be safe in preclinical models and sometimes early – stage human trials; there can also be a reduced time frame for drug development and less investment may be needed for development or testing. Repurposing existing drugs as MDM2 inhibitors through computational methods can provide a more significant number of drug candidates.

In this work, we evaluated the binding conformation of the compounds in the DrugBank database as repurposed MDM2 inhibitors through Molecular Docking and Molecular Dynamics (MD) simulations.

2 Experimental Methods

2.1 Molecular Docking

Multiple crystal structures of MDM2 (PDB ID: 1YCR, 1RV1, 1T4E, 2GV2, 3JZR, 3JZS, 3LBK, 3TJ2, 3VZV) were obtained from the RCSB Protein Data Bank to obtain an ensemble of MDM2 structure conformation with an open ligand cavity.

The crystal structures were super-imposed and hydrogenated using the Genetic Optimization for Ligand Docking (GOLD) 5.3.0 software[10]. The crystal structure of p53 obtained from the 1YCR's binding site was used as the reference binding site and defined as a 6 Å radius sphere around the ensemble of MDM2.

The GoldScore, ChemScore, and ChemPLP scoring functions implemented in GOLD were used to determine the top-scoring docked poses of the compounds. The docking poses were visualized using PyMol[11].

A Receiver Operating Characteristic (ROC) curve was plotted to evaluate the performance of our MDM2 inhibitor dockings. A consensus scoring was used for the multiple scoring functions to balance out the errors of individual scoring functions. The consensus score was obtained by normalizing the values of each score, as shown in the equation below.

$$\text{Mean normalized value} = \frac{\text{original docking score} - \text{sample mean}}{\text{maximum docking score} - \text{minimum docking score}}$$

The consensus score was calculated by taking the summation of the three different docking functions.

2.2 Molecular Dynamics (MD) simulations

MD simulations and binding free energies were performed via AMBER20. To prepare the system, the antechamber module was employed for each individual ligand to create their topology files, followed by assigning GAFF ligand forcefield parameter with the *tleap* module[12]. In contrast, the *ff19SB* force field was applied to the MDM2 protein. After combining the ligand with the protein, each system was solvated in a truncated octahedron periodic box with water molecules distancing 10 Å on all sides using the TIP3P water model. Their charges were neutralized with Cl^- ions[13].

Two minimization stages were conducted for each protein-ligand complex, followed by heating, equilibration, and production stages. During the initial step, 5000 steps of steep descent followed by 5000 conjugate gradient minimizations were executed with 300 kcal mol^{-1} restraint force on the complex, a maximum of 10,000 minimization cycles, and 10 Å PME non-bonded cutoff distance. Thereafter, the systems were engaged in 100,000 steps of steepest descent in succession to 10,000 conjugate gradient minimizations with a maximum of 20,000 minimization cycles and the same PME cutoff distance. To run an NVT ensemble, the complexes were then heated from 0 to 300 K; the temperatures were controlled with a Langevin thermostat, while the pressure was controlled at 1 bar with the Berendsen barostat. After heating, 5 ns of equilibration stage via NPT ensemble followed by 250 ns of production stage were taken place while maintaining the temperature at 300 K and constraining fast motion bond involving hydrogen atoms using the SHAKE algorithm.

The trajectory analysis of the complexes (RMSD, RGyr and RMSF) was done using the *cpptraj* module as seen in AMBER20 by using a total of 62,500 frames from the 250 ns simulations[14]. The RGyr of the binding pocket residues of MDM2 was calculated with the residues that are in 8 Å radius from the ligand binding site of the docked poses (residues: Met50-Tyr76 and Phe91-Ile103). The free binding energies of the protein-ligand complex were calculated from a 250 snapshot of the final 10 ns of the simulation with the *MMPBSA.py* module of the AMBER20[15].

3 Results and Discussions

3.1 Molecular Docking

The scoring functions used in this experiment are categorized as 'Empirical Scoring Functions', estimating the binding affinity of the complex and ranking the complex structure candidates – the highest ranked structures are used[16].

Each scoring function models the structure differently, ChemScore estimates total free energy on binding, ChemPLP assesses the steric complementarity, and GoldScore combines force-fields: hydrogen bonds, van der Waals energy, metal interactions, and torsion deformations[16]. Consensus scoring allows multiple scoring functions to be used simultaneously and can avoid any pitfalls or disadvantages posed by individual scoring functions[16,17].

From our docking of known ligands (Active: 41 compounds, Inactive: 171 compounds), the GoldScore achieved an Area Under the Receiver Operator Characteristic (ROC) of 0.65, ChemScore achieved a ROC of 0.61 and ChemPLP achieved a ROC of 0.61, and the consensus scoring of all three scoring functions achieved a ROC of 0.70 (Figure 1).

The advantage of consensus scoring can be seen in the ROC curves (Figure 1; Supplementary Table ST1) during protocol optimization with MDM2 inhibitors. The consensus ROC achieved a sensitivity of 0.70, instead of the lower score ROC when calculated for individual scores[18]. From our docking of 513 DrugBank compounds, the DrugBank compounds scored similarly to the MDM2 inhibitors. In the case of Venetoclax, it showed the highest consensus docking score (Table 1). Meanwhile, both Timcodar and Phaeophytin-B also showed favourable docking scores (Table 1). The docked poses are shown in Supplementary Figure S1.

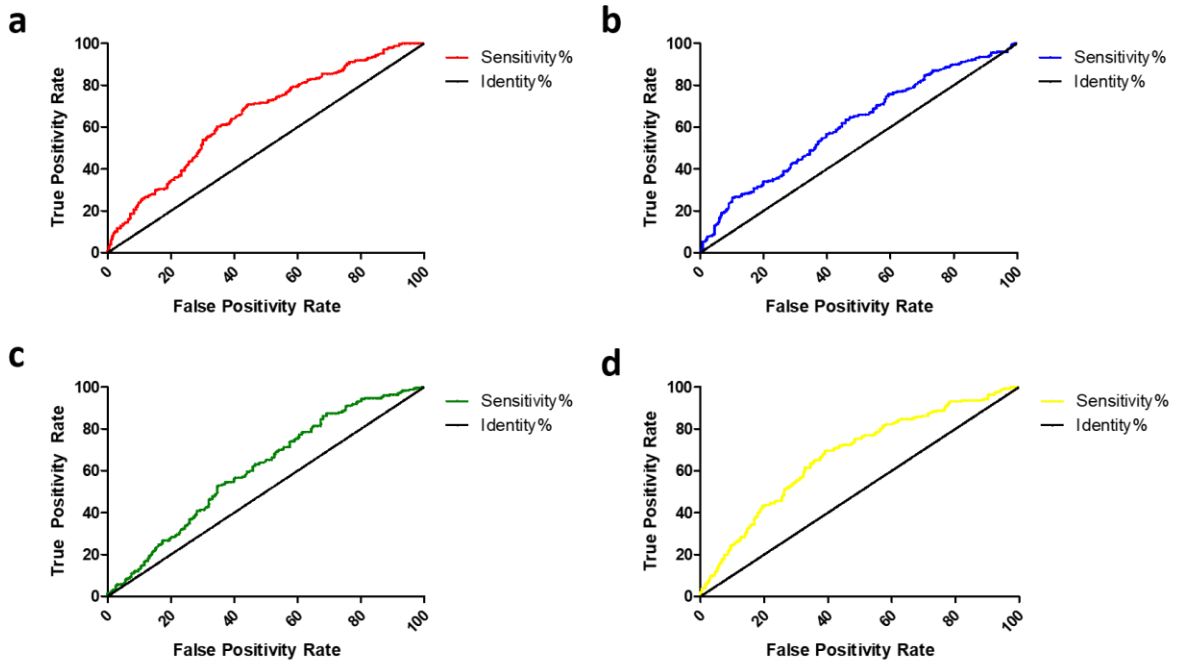

Figure 1. ROC curve of scoring functions. (a) ROC of GoldScore, (b) ROC of ChemScore, (c) ROC of CHEMPLP, and (d) ROC of consensus scoring.

Table 1. The docking scores of the top 10 compounds docked. The three chosen compounds for Molecular Dynamics simulations are shown in bold.

DrugBank ID	Compound name	GoldScore	ChemScore	ChemPLP	Consensus score
DB11581	**Venetoclax**	91.33	45.81	111.48	2.93
DB12761	**Timcodar**	81.37	42.29	98.38	2.47
DB04506	**Phaeophytin-B (1)***	74.16	42.87	99.33	2.37
DB04506	Phaeophytin-B (2)*	73.45	42.13	100.82	2.36
DB12138	PF-03715455	71.95	38.55	95.82	2.19
DB06494	Sufugolix	80.33	36.65	86.12	2.15
DB06638	Quarfloxin (1)**	66.77	40.20	97.61	2.15
DB12037	Vedropevir	78.51	31.91	93.72	2.14
DB02633	Cibacron blue	83.82	30.86	87.50	2.12
DB06638	Quarfloxin (2)**	75.18	39.04	86.63	2.12

*Isomers of Phaeophytin-B
**Isomers of Quarfloxin

Venetoclax is a Bcl-2 inhibitor used to treat chronic lymphocytic leukemia (CLL), small lymphocytic lymphoma (SLL), or acute myeloid leukemia (AML). Synergistic activity was observed with Venetoclax and the MDM2 inhibitor, Idasanutlin on AML, and neuroblastoma cell lines[19,20]. These studies have shown the synergistic effect of Venetoclax and Idasanutlin on cancer cell lines with Bcl-2 expression. However, EBV infection has been found to have low Bcl-2 expression – the main target of Venetoclax[20].

Phaeophytin-B is a natural pigment molecule derived from chlorophyll[21]. Previous studies have shown anti-tumour activity of Phaeophytin-B by effectively suppressing tumour promotion in mammals[22]. Additionally, it has demonstrated the ability to suppress the production of cytokines by mammalian macrophages, including humans[23].

Meanwhile, Timcodar is a benzenepropanamide derivative that is currently under investigation for studying of adult solid tumours. Timcodar had demonstrated the improvement of potency

of antimycobacterial agents, including antituberculosis (anti-TB) drugs by acting as an efflux pump inhibitor[24].

3.2 *Molecular Dynamics (MD) Simulations*

Following the results of molecular docking, we identified three compounds, Venetoclax, Timcodar and Phaeophytin-B (Figure 2a-c), to further study the potential binding mechanisms through MD simulations due to their good consensus docking scores. The MDM2-docked pose of the three compounds and the MDM2 in its apo-state were subjected to 250 ns of simulation; from the simulation, the Root Mean Square Deviation (RMSD) and the Radius of Gyration (RGyr), Root Mean Square Fluctuation (RMSF) were calculated. Additionally, we simulated a known MDM2 inhibitor, CHEMBL3908421 (Control) that exhibited the highest docking consensus score from the known MDM2 inhibitor docking (Supplementary Table ST1).

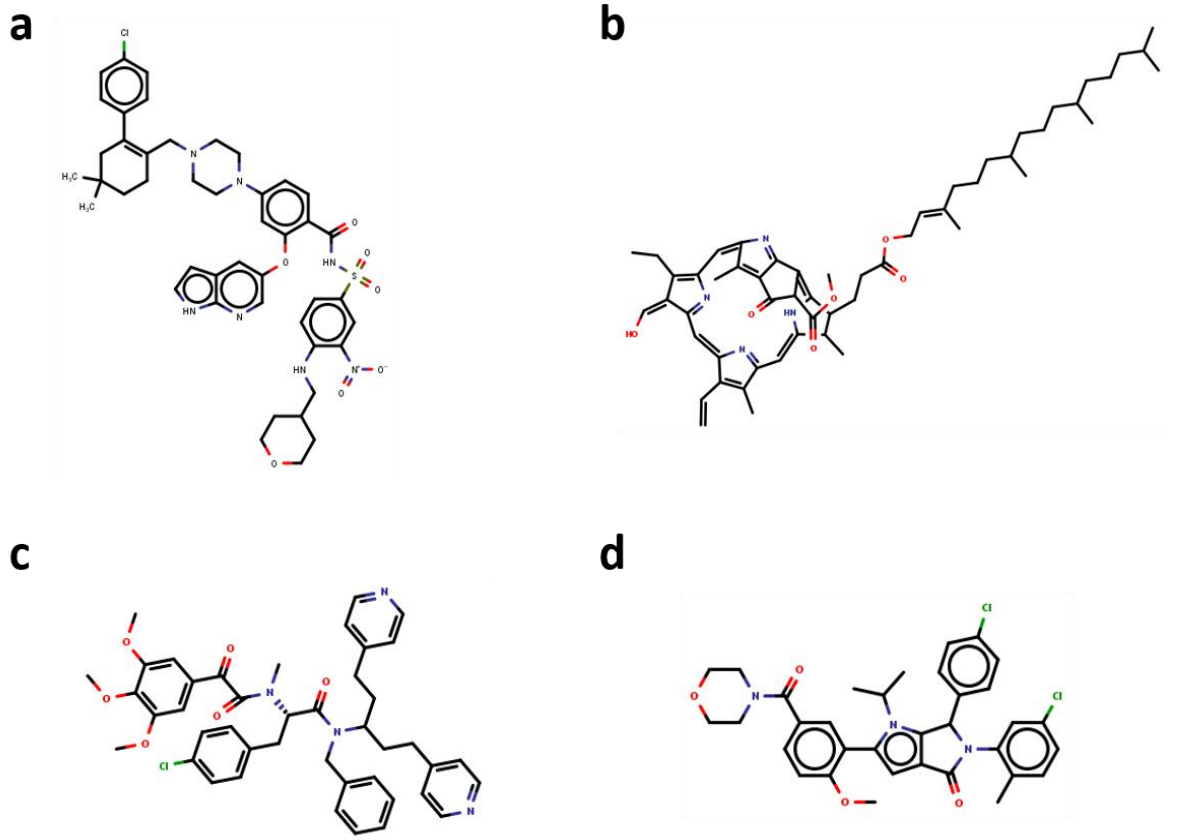

Figure 2. Chosen chemical structures of the ligands after docking. (a) Venetoclax, (b) Phaeophytin-B, (c) Timcodar and (d) CHEMBL3908421 (Control).

The average RMSD of MDM2 as a whole in the apo-state and the complexes spanned between 1.15 Å and 1.66 Å. The Venetoclax-MDM2 complex reached stability at 140 ns-mark with an average RMSD of 1.48 Å (Figure 3a). The Phaeophytin-B-MDM2 complex and the apo-state maintained stability throughout 250 ns of simulation with average RMSD being 1.38 Å and 1.66 Å, respectively (Figure 3b and e). Meanwhile, Timcodar-MDM2 complex reached stability at around the 100 ns-mark, with an average RMSD of 1.46 Å (Figure 3c). The protein RMSD of the CHEMBL3908421-MDM2 complex showed stability throughout the simulation with an average RMSD of 1.21 Å (Figure 3d). In all cases, the residues of the binding pockets also reached stability (Supplementary Figure S2).

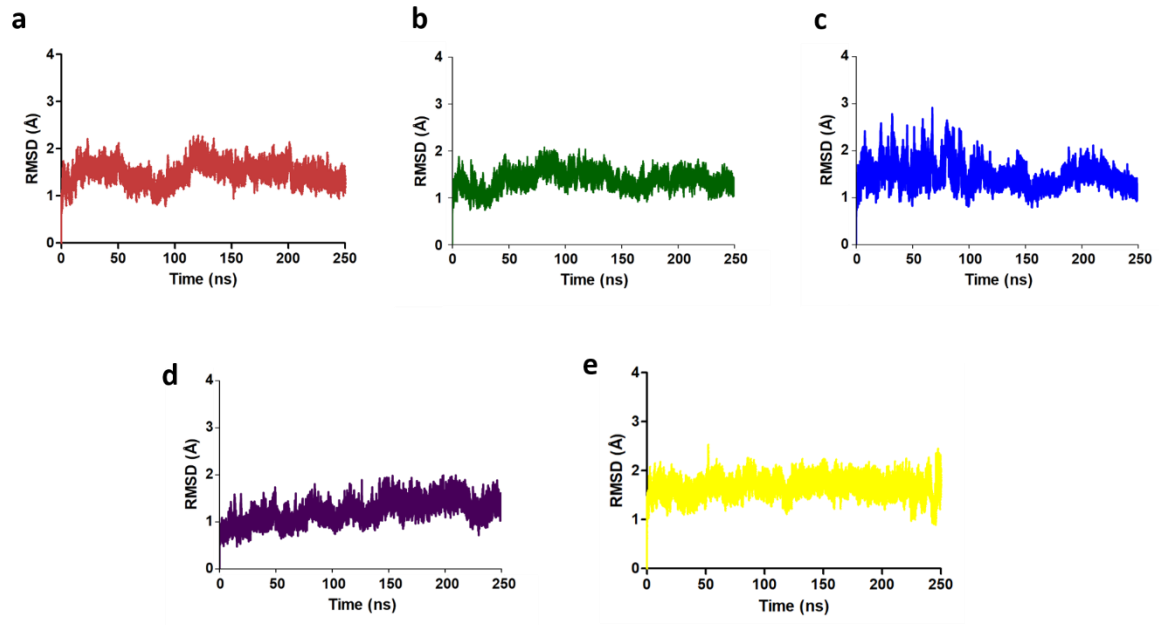

Figure 3. RMSD of MDM2 as a whole. (a) RMSD of the Venetoclax-MDM2 complex, (b) RMSD of the Phaeophytin-B-MDM2 complex, (c) RMSD of Timcodar-MDM2 complex, (d) RMSD of the CHEMBL3908421-MDM2 complex and (e) RMSD of the MDM2 in apo-state.

Meanwhile, the average RMSD of our ligands, Venetoclax, Phaeophytin-B, Timcodar, and the CHEMBL3908421 (henceforth referred to as ligands), spanned between 1.80 Å and 4.83 Å (Figure 4). Venetoclax reached stability at around the 10 ns mark, with a spike at around 160 ns but reaching stability with an average RMSD of 3.99 Å (Figure 4a). Phaeophytin-B showed a relatively low average RMSD of 2.21 Å upon reaching the 10 ns-mark (Figure 4b). Although Timcodar showed an average RMSD of 4.83 Å throughout the simulation, it did not attain stability with the RMSD reaching up to 9.92 Å (Figure 4c). CHEMBL3908421 showed the lowest average RMSD with 1.80 Å throughout the simulation (Figure 4d). A high ligand RMSD fluctuation of more than 2 Å would indicate ligand binding instability[25]. In the case of Venetoclax and Phaeophytin-B, they both showed stability in binding to the binding pocket of MDM2 with low fluctuations. The initial deviation of Venetoclax and Phaeophytin-B is due to slight rearrangements that take place within the binding pocket (Figure 5).

Next, we assessed the RGyr of the binding site to observe the compactness of our complexes and MDM2 in its apo-state (Figure 6). The binding site compactness of Venetoclax-MDM2, Phaeophytin-B-MDM2, and Timcodar-MDM2 maintained stability throughout the simulation with the average of 11.91 Å, 11.97 Å and 11.75 Å, respectively (Figure 6a-c). Meanwhile, both CHEMBL3908421-MDM2 and MDM2 in apo-state showed an average RGyr of 11.72 Å and 11.93 Å, respectively (Figure 6d and e).

Lastly, we calculated the RMSF of the amino acids of the complexes (Figure 7a-e) as a part of our trajectory analysis. In all complexes, the highest RMSF was seen for Glu25 and Val109. Additionally, Lys70 in the Venetoclax-MDM2 complex showed high RMSF in comparison to the lower RMSFs in the Phaeophytin-B-MDM2, Timcodar-MDM2 and the CHEMBL3908421-MDM2 complexes (Figure 7a-d). All of the residues of the MDM2-Venetoclax (Figure 7a) complex displayed a significant increase compared to the MDM2 in apo-state (Figure 7e). These higher RMSF of the residues indicate increased global flexibility and conformational changes of the MDM2 protein. The Phaeophytin-B-MDM2, Timcodar-MDM2 and the CHEMBL3908421-MDM2 complexes displayed similar RMSF compared to

MDM2 in apo-state (Figure 7b-e). This shows that Phaeophytin-B, Timcodar and CHEMBL390842 binding to MDM2 does not cause high fluctuations, resulting in binding site conformational stability. These two behaviours of our complexes are attributed to conserved MDM2, yet a flexible binding site. The MDM2 binding site forms the hydrophobic pocket found in MDM2-p53 binding but varying flexibility has also been observed after p53 and other ligands are bound to MDM2[26,27].

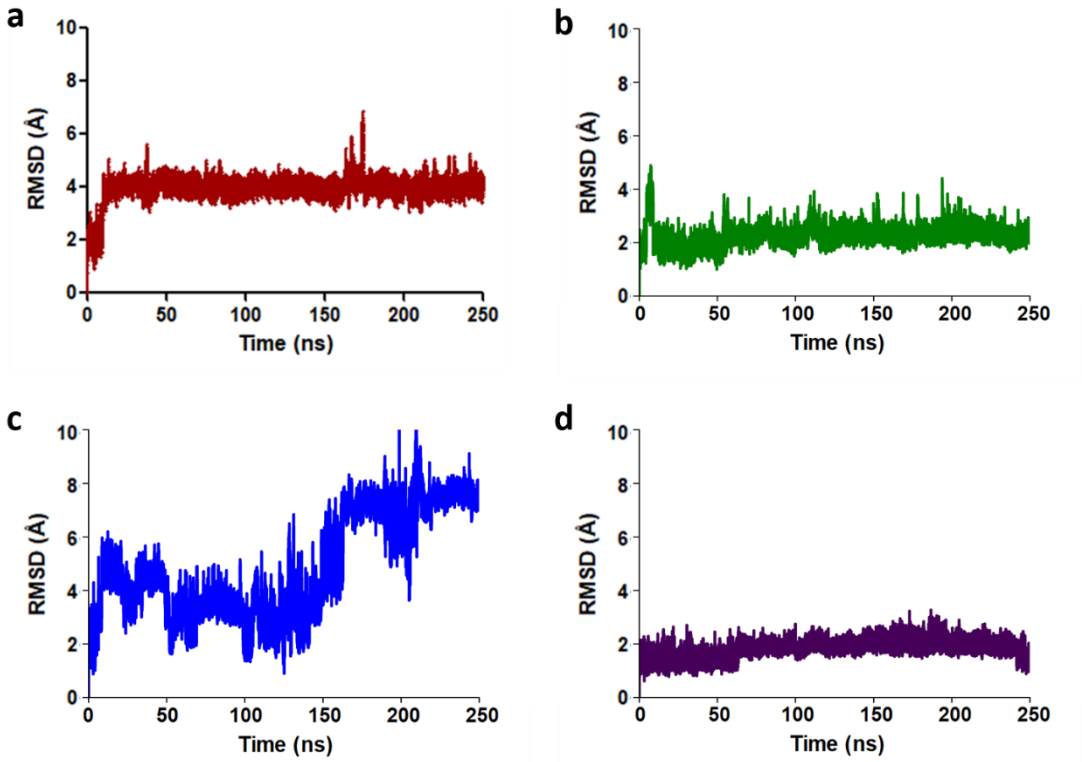

Figure 4. RMSD of the ligands. (a) RMSD of Venetoclax, (b) RMSD of Phaeophytin-B, (c) RMSD of Timcodar and (d) RMSD of CHEMBL3908421 (Control).

3.3 Protein-Ligand Interaction & MM-GBSA Calculations

As the next stage, we calculated the protein-ligand interaction and binding free energies to further investigate the binding stability of our complexes further the MM-GBSA method using the final 10 ns of the simulations[15]. Both Venetoclax and Phaeophytin-B showed higher binding free – energies of –50.46 kcal mol^{-1} and –50.86 kcal mol^{-1} in comparison to the control inhibitor, CHEMBL3908421 (Binding energy: –34.67 kcal mol^{-1}) (Table 2). Meanwhile, Timcodar exhibited similar binding free energy to the control inhibitor (Binding energy: –37.93 kcal mol^{-1}) (Table 2). In all cases, the MDM2-ligand interactions were favoured through the Van der Waals energy (VDWaal) energy contribution (Table 2). This showed that the interactions between the ligands and MDM2 were dominated through hydrophobic interactions. These hydrophobic interactions hinted that our predicted pose relies on the deep hydrophobic cleft of MDM2, found between the α2 helix and middle β sheet[26].

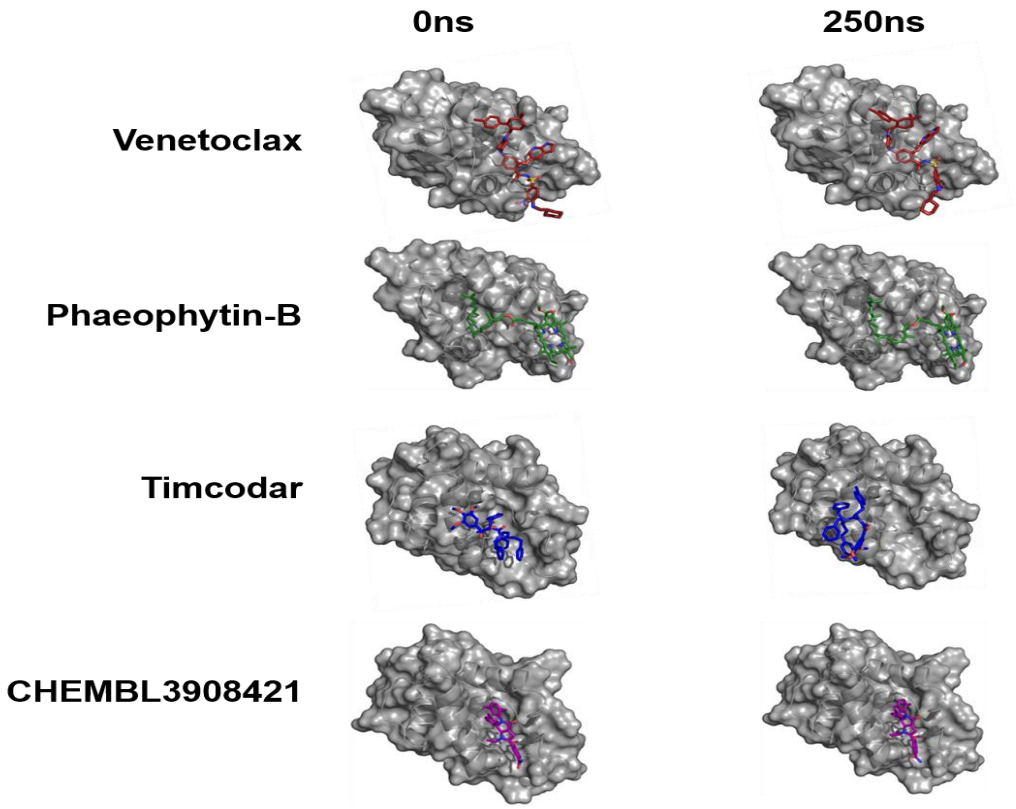

Figure 5. The initial (0 ns) and the final (250 ns) frames of each simulation of Venetoclax, Timcodar, Phaeophytin-B and CHEMBL3908421. Venetoclax, Phaeophytin-B, Timcodar, and CHEMBL3908421 are shown in red, green, blue, and purple, respectively. The protein surface is shown in grey.

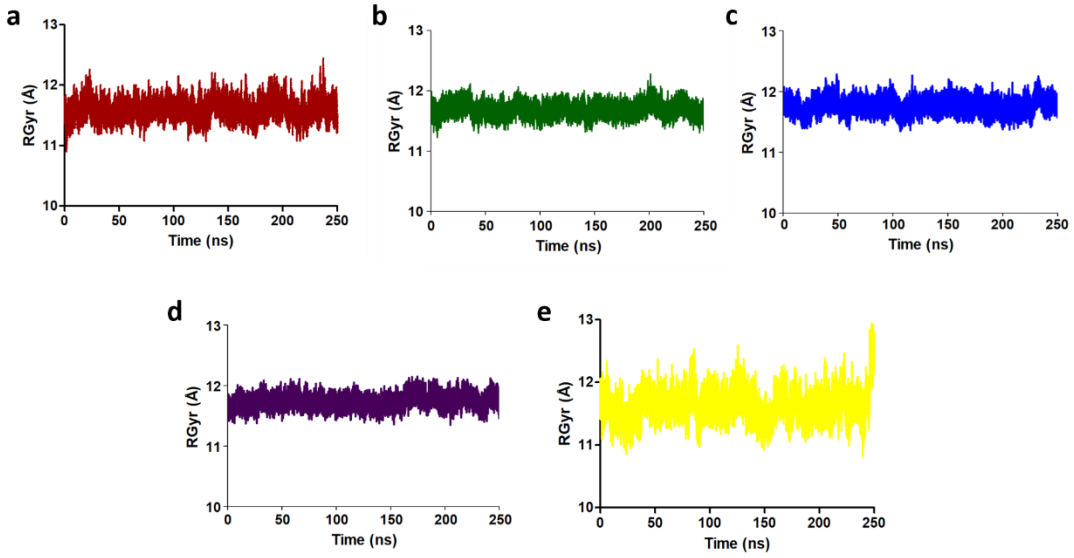

Figure 6. RGyr of binding site residues. (a) Binding site RGyr of Venetoclax-MDM2 complex, (b) Binding site RGyr of Phaeophytin-B-MDM2 complex, (c) Binding site RGyr of Timcodar-MDM2 complex, (d) Binding site RGyr of the CHEMBL3908421-MDM2 complex and (e) Binding site RGyr of MDM2 in its apo-state.

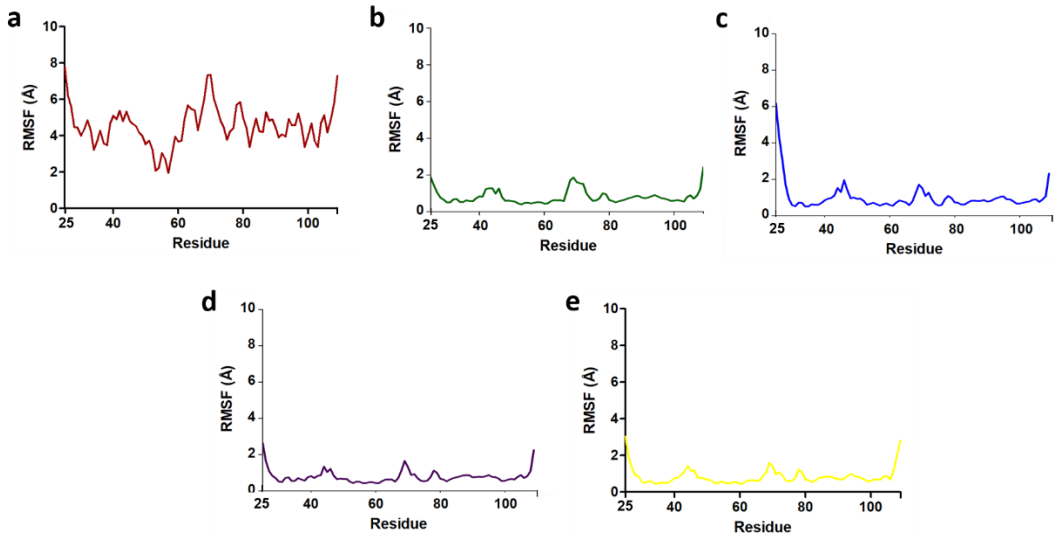

Figure 7. RMSF of the residues of MDM2 in apo-state and in complexes. (a) RMSF of Venetoclax-MDM2 complex, (b) RMSF of Phaeophytin-B-MDM2 complex, (c) RMSF of Timcodar-MDM2 complex, (d) RMSF of the CHEMBL3908421-MDM2 complex and (e) RMSF of MDM2 in its apo-state.

Table 2. Binding affinities Venetoclax, Phaeophytin-B, Timcodar, and CHEMBL3908421 (Control) with MDM2. Energy components are presented in kcal mol^{-1} with their standard deviation.

Energy component (kcal mol^{-1})	Venetoclax	Phaeophytin-B	Timcodar	CHEMBL3908421
ΔE_{vdw}	–66.81 ± 2.72	–65.08 ± 4.08	–49.67 ± 6.23	–42.52 ± 2.96
ΔE_{ele}	–15.09 ± 1.79	–6.85 ± 3.83	–8.91 ± 6.58	–12.76 ± 4.53
ΔE_{polar}	40.03 ± 1.66	29.06 ± 3.16	26.97 ± 5.53	26.26 ± 4.40
$\Delta E_{non\text{-}polar}$	–8.59 ± 0.15	–7.97 ± 0.53	–6.32 ± 0.71	–5.64 ± 0.31
ΔG_{gas}	–81.90 ± 4.07	–71.94 ± 4.51	–58.59 ± 8.62	–55.29 ± 5.25
ΔG_{sol}	31.44 ± 1.54	21.08 ± 3.25	20.67 ± 5.21	20.62 ± 4.29
ΔG_{total}	–50.46 ± 3.55	–50.86 ± 3.41	–37.93 ± 5.20	–34.67 ± 2.40

Next, we opted to calculate the energy contribution per residue for each complex. We considered the residues that contributed largely (< –1 kcal mol^{-1}) towards the ligand-MDM2 interaction. The highest contributions for the interaction between Venetoclax and MDM2 were seen for residues Gln59, Met62, Gly58, Phe55 and Gln72 (Figure 8a). In the case of Phaeophytin-B-MDM2 interaction, the highest contributions were seen for residues Lys51, Phe55, Leu54, Glu52, Thr49, Ile61, Ile99 and Val93 (Figure 8b). Meanwhile, the highest contributions were seen by Leu54, Phe55, Ile61 and Val69 for the Timcodar-MDM2 complex (Figure 8c). CHEMBL3908421-MDM2 interaction showed high energy contributions by the residues, Leu54, Ile61, Met62 and Val93 (Figure 8d). Our ligands Phaeophytin-B and Timcodar interact with key residues in the MDM2 N-terminal region and share residue binding of the p53-MDM2 complex and other MDM2-Inhibitor complexes; these key residues are Leu54, Leu57, Ile61, and Val93 (Figure 9a-d)[28-33]. It is noteworthy that Venetoclax did not show significant binding interactions with the aforementioned key residues of MDM2.

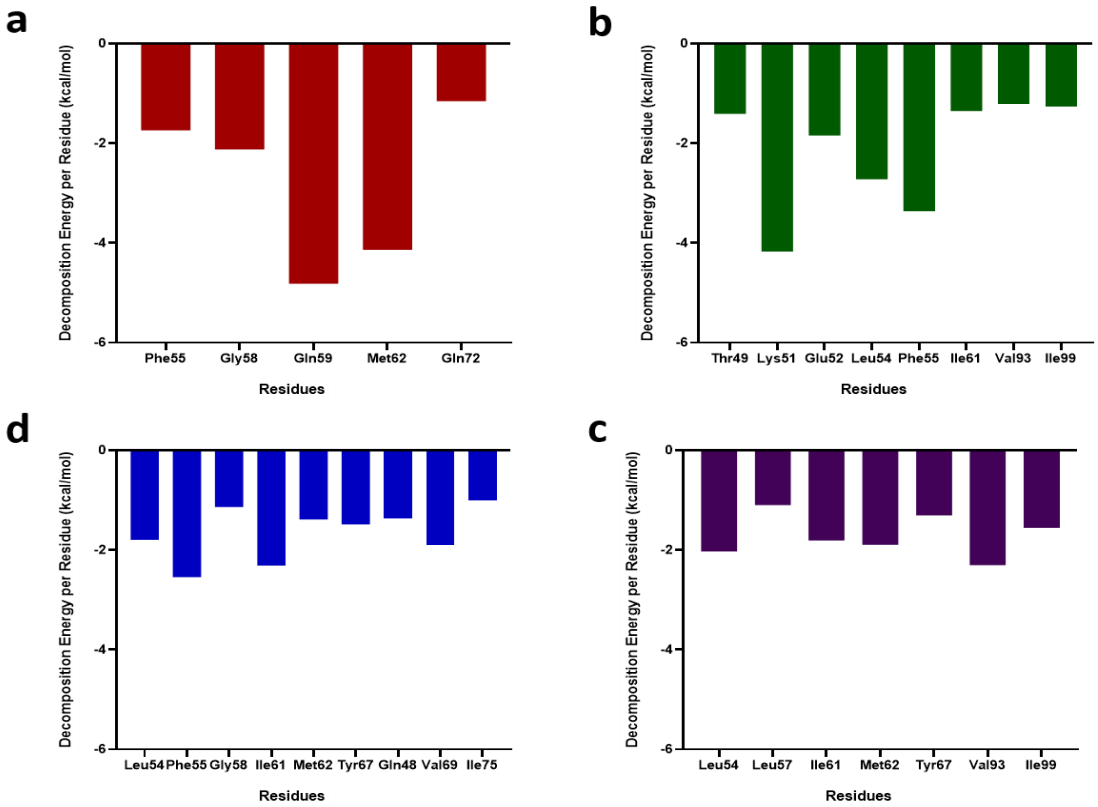

Figure 8. The top (< –1 kcal mol^{-1}) residues of MDM2 that interact with (a) Venetoclax, (b) Phaeophytin-B, (c) Timcodar and (d) CHEMBL3908421.

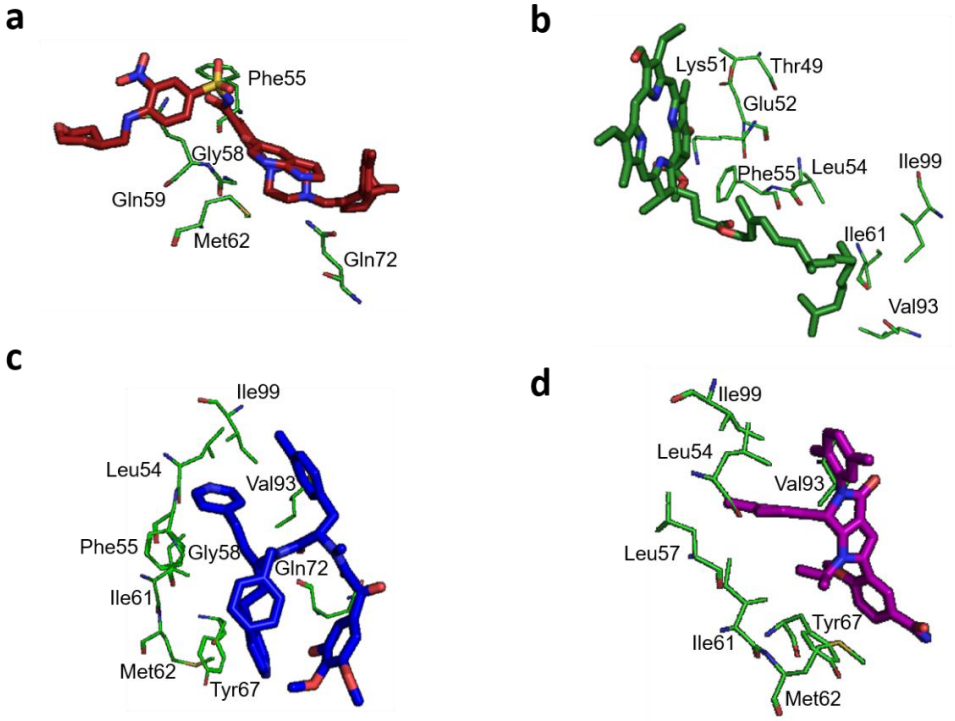

Figure 9. The key residues of MDM2 that interact with the ligands. (a) The residues that interact with Venetoclax, (b) The residues that interact with Phaeophytin-B, (c) The residues that interact with Timcodar and (d) The residues that interact with CHEMBL3908421 (Control). The structures are extracted from the final frame of each simulation.

4 Conclusion

The MDM2 protein is found to be disrupted by being excessively upregulating p53 due to infection by the Epstein-Barr Virus (EBV), which can lead to Nasopharyngeal cancer – the fifth most common cancer in Malaysia among males aged between 25-59. We searched for potential MDM2 inhibitor candidates through the DrugBank catalogue of existing compounds, and we performed molecular docking to identify potential poses with MDM2. The top three scoring compounds, Venetoclax, Timcodar and Phaeophytin-B, were further investigated by conducting 250 ns simulation of molecular dynamics to assess their binding stability and protein-ligand interactions. The results of our investigation led to the stable conformation of two ligands docked with MDM2: Venetoclax and Phaeophytin-B. Our MM-GBSA calculations of Venetoclax and Phaeophytin-B showed that the interactions are favoured through hydrophobic interactions. We conclude that Venetoclax and Phaeophytin-B could be potential chemical scaffolds for future rational drug design of MDM2 inhibitors based on their binding stability with MDM2.

Conflict of Interest

The authors declare no conflicting interests.

Supplementary Material

The Supporting file is available free of charge at https://docs.google.com/document/d/190-3rERjuVl56IVA4OfygEYmD5vmi_0Z/edit?usp=sharing&ouid=107515533382608139091&rtpof=true&sd=true

Acknowledgment

The authors would like to thank the editors and the reviewers for their valuable suggestions to improve the manuscript.

Funding

The authors received no funding for this study.

Author Contribution

Conceptualization: Chee, X.W.
Data curation: Gunasinghe, J., Abu Talib, M.I., & Cheah, S.
Methodology: Chee, X.W.
Formal analysis: Gunasinghe, J., Abu Talib, M.I., & S. Cheah
Visualisation: Gunasinghe, J., Abu Talib, M.I., & S. Cheah
Software: J. Gunasinghe, Abu Talib, M.I.
Writing (original draft): Gunasinghe, J., Abu Talib, M.I., & S. Cheah
Writing (review and editing): Gunasinghe, J., Abu Talib, M.I., S. Cheah, I.R. Ginjom, Lee, S.H., & Chee, X.W.
Validation: Gunasinghe, J., & Chee, X.W.
Supervision: Chee, X.W.
Funding acquisition: Not applicable
Project administration: Chee, X.W.

References

1. Sung, H., Ferlay, J., Siegel, R. L., Laversanne, M., Soerjomataram, I., Jemal, A., & Bray, F. (2021). Global cancer statistics 2020: GLOBOCAN estimates of incidence and mortality worldwide for 36 cancers in 185 countries. *Cancer Journal for Children, 71*(3), 209-249. https://doi.org/10.3322/caac.21660
2. Devi, B. C. R., Pisani, P., Tang, T. S., & Parkin, D. M. (2004). High incidence of nasopharyngeal carcinoma in native people of Sarawak, Borneo Island. *Cancer Epidemiol Biomarkers and Prevention, 13*(3), 482-486. https://doi.org/10.1158/1055-9965.482.13.3
3. Chang, E. T., Ye, W., Zeng, Y. X., & Adami, H. O. (2021). The evolving epidemiology of nasopharyngeal carcinoma. *Cancer Epidemiology, Biomarkers and Prevention*, *30*(6), 1035-1047. https://doi.org/10.1158/1055-9965.EPI-20-1702.
4. Arvin, A., Campadelli-Fiume, G., Mocarski, E., S.Moore, P., Roizman, B., Whitley, R., & Yamanishi, K. (2007). *Human herpesviruses: Biology, therapy, and immunoprophylaxis*. Cambridge University Press. https://doi.org/10.1017/CBO9780511545313
5. Wu, H. C., Lu, T. Y., Lee, J. J., Hwang, J. K., Lin, Y. J., Wang, C. K. & Lin, C. T. (2004). MDM2 expression in EBV-infected nasopharyngeal carcinoma cells. *Laboratory Investigation*, *84*, 1547-1556. https://doi.org/10.1038/labinvest.3700183
6. Forte, E. & Luftig, M. A. (2009). MDM2-Dependent inhibition of P53 is required for Epstein-Barr virus B-cell growth transformation and infected-cell survival. *Journal of Virology, 83*(6), 2491-2499. https://doi.org/10.1128/JVI.01681-08

7. Zhang, X., Zhang, R., Ren, C., Xu, Y., Wu, S., Meng, C., Pataer, A., Song, X., Yao, Y., He, H., Chen, H., Wang, J., Meric-Bernstam, F., Champlin, R. E., Heymach, J. V., Rooney, C. M., Swisher, S. G., Vaporciyan, A. A., Roth, J. A., You, M. J., Wang, M., & Fang, B. (2022). Epstein Barr virus–positive B-cell lymphoma is highly vulnerable to MDM2 inhibitors *in vivo*. *Blood Advances*, *6*(3), 891-901. https://doi.org/10.1182/bloodadvances.2021006156
8. Shangary, S., & Wang, S. (2008). Targeting the MDM2-P53 *Interaction for Cancer Therapy*. *Clinical Cancer Research*, *14*(17), 5318-5324. https://doi.org/10.1158/1078-0432.CCR-07-5136
9. Pushpakom, S., Lorio, F., Eyers, P. A., Escott, K. J., Hopper, S., Wells, A., Doig, A., Guilliams, T., Latimer, J., McNamee, C., Norris, A., Sanseau, P., Cavalla, D., & Pirmohamed, M. (2019). Drug repurposing: Progress, challenges and recommendations. *Nature Reviews Drug Discovery, 18*(1), 41-58. https://doi.org/10.1038/nrd.2018.168
10. Jones, G., Willett, P., Glen, R. C., Leach, A. R., & Taylor, R. (1997). Development and validation of a genetic algorithm for flexible docking. *Journal of Molecular Biology*, *267*(3), 727-748. https://doi.org/10.1006/jmbi.1996.0897
11. Yuan, S., Chan, H. C. S., & Hu, Z. (2017). Using PyMOL as a platform for computational drug design. *WIREs Computational Molecular Science*, *7*(2), e1298. https://doi.org/10.1002/wcms.1298
12. Alviz-Amador, A., Galindo-Murillo, R., Pérez-González, H., Rodríguez-Cavallo, E., Vivas-Reyes, R., & Méndez-Cuadro, D. (2020). AMBER Parameters and topology data of 2-pentylpyrrole adduct of arginine with 4-hydroxy-2-nonenal. *Journal Data in Brief, 29*, 105294. https://doi.org/10.1016/j.dib.2020.105294
13. Jorgensen, W. L., Chandrasekhar, J., Madura, J. D., Impey, R. W. & Klein, M. L. (1983). Comparison of simple potential functions for simulating liquid water. *Journal of Chemical Physics, 79*(2), 926-935. https://doi.org/10.1063/1.445869
14. Roe, D. R., & Cheatham, T. E. (2013). PTRAJ and CPPTRAJ: Software for processing and analysis of molecular dynamics trajectory data. *Journal of Chemical Theory and Computation, 9*(7), 3084-3095. https://doi.org/10.1021/ct400341p
15. Genheden, S., & Ryde, U. (2015). The MM/PBSA and MM/GBSA methods to estimate ligand-binding affinities. *Journal of Expert Opinion and Drug Discov*ery, *10*(5), 449-461. https://doi.org/10.1517/17460441.2015.1032936
16. Sapundzhi, F., Prodanova, K., & Lazarova, M. (2019, June 7-13). *Survey of the scoring functions for protein-ligand docking*. The 45th International Conference on Application of Mathematics in Engineering and Economics, Sozopol, Bulgaria. https://doi.org/10.1063/1.5133601
17. Oda, A., Tsuchida, K., Takakura, T., Yamaotsu, N., & Hirono, S. (2006). Comparison of consensus scoring strategies for evaluating computational models of protein−ligand complexes. *Journal of Chemical Information and Modeling*, *46*(1), 380-391. https://doi.org/10.1021/ci050283k
18. Hanley, J. A., & McNeil, B. J. (1982). The meaning and use of the area under a receiver operating characteristic (ROC) curve. *Radiology*, *143*(1), 29-36. https://doi.org/10.1148/radiology.143.1.7063747
19. Goethem, A. V., Yigit, N., Moreno-Smith, M., Vasudevan, S. A., Barbieri, E., Speleman, F., Shohet, J., Vandesompele, J., & Maerken, T. V. (2017). Dual targeting of MDM2 and BCL2 as a therapeutic strategy in neuroblastoma. *Oncotarget*, *8*(34), 57047-57057. https://doi.org/10.18632/oncotarget.18982
20. Lehmann, C., Friess, T., Birzele, F., Kiialainen, A., & Dangl, M. (2016). Superior anti-tumor activity of the MDM2 antagonist idasanutlin and the Bcl-2 inhibitor venetoclax in P53 wild-type acute myeloid leukemia models. *Journal of Hematology and Oncology*, *9*, 50. https://doi.org/10.1186/s13045-016-0280-3
21. Li, X., Zhou, R., Xu, K., Xu, J., Jin, J., Fang, H., & He, Y. (2018). Rapid determination of chlorophyll and pheophytin in green tea using fourier transform infrared spectroscopy. *Journal of Molecules*, *23*(5), 1-13. https://doi.org/10.3390/molecules23051010
22. Higashi-Okai, K., Otani, S., & Okai, Y. (1998). Potent suppressive activity of pheophytin a and b from the non-polyphenolic fraction of green tea (camellia sinensis) against tumor promotion in mouse skin. *Cancer Letters*, *129*(2), 223-228. https://doi.org/10.1016/S0304-3835(98)00113-X
23. Lin, C. Y., Wang, W. H., Chen, S.H., Chang, Y.W., Hung, L. C., Chen, C. Y., & Chen, Y. H. (2017). lipopolysaccharide-induced nitric oxide, prostaglandin E2, and cytokine production of mouse and human macrophages are suppressed by pheophytin-b. *International Journal of Molecular Sciences, 18*(12), 2637. https://doi.org/10.3390/ijms18122637
24. Grossman, T. H., Shoen, C. M., Jones, S. M., Jones, P. L., Cynamon, M. H., & Locher, C. P. (2015). The efflux pump inhibitor timcodar improves the potency of antimycobacterial agents. *Journal of Antimicrobial Agents and Chemotherapy*, *59*(3), 1534-1541. https://doi.org/10.1128/AAC.04271-14

25. Knapp, B., Frantal, S., Cibena, M., Schreiner, W., & Bauer, P. (2011). Is an intuitive convergence definition of molecular dynamics simulations solely based on the root mean square deviation possible? *Journal of Computational Biology*, *18*(8), 997-1005. https://doi.org/10.1089/cmb.2010.0237
26. Bueren-Calabuig, J. A. & Michel, J. (2015). Elucidation of ligand-dependent modulation of disorder-order transitions in the oncoprotein MDM2. *PLOS Computational Biology*, *11*(6), 1-27. https://doi.org/10.1371/journal.pcbi.1004282
27. Kussie, P. H., Gorina, S., Marechal, V., Elenbaas, B., Moreau, J., Levine, A. J., Pavletich, N. P. (1996). Structure of the MDM2 oncoprotein bound to the P53 tumor suppressor transactivation domain. *Journal of Science*, *274*(5289), 948-953. https://doi.org/10.1126/science.274.5289.948
28. Estrada-Ortiz, N., Neochoritis, C. G., & Dömling, A. (2016). How to design a successful P53-MDM2/X interaction inhibitor: A thorough overview based on crystal structures. *ChemMedChem*, *11*(8), 757-772. https://doi.org/10.1002/cmdc.201500487
29. Gureev, M., Novikova, D., Grigoreva, T., Vorona, S., Garabadzhiu, A., & Tribulovich, V. (2020). Simulation of MDM2 N-Terminal domain conformational lability in the presence of imidazoline based inhibitors of MDM2-P53 protein–protein interaction. *Journal of Computer-Aided Molecular Design*, *34*(1), 55-70. https://doi.org/10.1007/s10822-019-00260-6
30. Munisamy, M., Mukherjee, N., Thomas, L., Pham, A. T., Shakeri, A., Zhao, Y., Kolesar, J., Rao, P. P. N., Rangnekar, V. M., & Rao, M. (2021). Therapeutic opportunities in cancer therapy: Targeting the P53-MDM2/MDMX interactions. *American Journal of Cancer Research*, *11*(12), 5762-5781.
31. Popowicz, G. M., Czarna, A., Wolf, S., Wang, K., Wang, W., Dömling, A., & Holak, T. A. (2010). Structures of low molecular weight inhibitors bound to MDMX and MDM2 reveal new approaches for P53-MDMX/MDM2 antagonist drug discovery. *Cell Cycle*, *9*(6), 1104-1111. https://doi.org/10.4161/cc.9.6.10956
32. Popowicz, G. M., Dömling, A., & Holak, T. A. (2011). The structure-based design of Mdm2/Mdmx–P53 inhibitors gets serious. *Angewandte Chemie*, *50*(12), 2680-2688. https://doi.org/10.1002/anie.201003863
33. Chen, J., Wang, J., Xu, B., Zhu, W., & Li, G. (2011). Insight into mechanism of small molecule inhibitors of the MDM2–P53 interaction: Molecular dynamics simulation and free energy analysis. *Journal of Molecular Graphic and Modelling*, *30*, 46-53. https://doi.org/10.1016/j.jmgm.2011.06.003